M&C 2017 - International Conference on Mathematics & Computational Methods Applied to Nuclear Science & Engineering, Jeju, Korea, April 16-20, 2017, on USB (2017)

Impact of Perturbed H_2O Thermal Scattering Data in OPAL Reactor Calculations

Lance Maul

Australian Nuclear Science and Technology Organisation, B. 40, Locked Bag 2001, Kirrawee DC NSW 2232, Australia.
University of New South Wales, NSW, Australia.
lancem@ansto.gov.au

Abstract – *The estimation of uncertainties induced onto reactor integral quantities produced by the simulation of a research reactor are presented here. The Total Monte Carlo approach has been used in recent years to estimate uncertainties in the nuclear data used to produce cross sections for neutron transport codes. A large set of perturbed thermal scattering data was employed in a Serpent model of a fresh and an equilibrium core of the OPAL Reactor and examination of the effect was conducted on various quantities, such as k_{eff}, and selected reaction rates. Standard errors of 179 pcm for k_{eff} and relative errors of 0.69% for ^{239}Pu fission rate were observed, in addition to other key quantities of interest.*

I. INTRODUCTION

When simulating radiation transport, both a simulation engine containing the transport physics and nuclear data about the system's constituent materials are required. In characterising fission reactor systems, the primary particle of interest is the neutron and its interactions with materials present in and around the core. Measurements of neutron-nucleus interactions have been taken for most isotopes and used to fine tune approximate models to predict interaction probability: the cross section. Most materials are generally of small importance or negligible impact for the purposes of simulating a fission reactor and a free gas approximation is satisfactory. There are, however, key materials that can play far more pivotal roles in influencing neutron behaviour; in thermal reactors, one important class of materials are the moderators. The energy of a thermalised neutron is the same order of magnitude as the binding energy of molecular bonding and the wavelength of the neutron is close to intermolecular distances [1]. This renders the free gas approximation unsuitable in this energy range for such materials as an incident thermal neutron can cause molecular excitations not addressed in the data.

To account for this, a treatment is applied to the cross section for key isotopes used in moderators called a thermal scattering law (TSL). This data governs the secondary energy and angle distributions a neutron is subject to after a scattering event with a given moderator material. A neutron can scatter via a few different mechanisms: inelastic scattering (important for all materials), incoherent elastic scattering (important for hydrogenous solids) and coherent elastic scattering (important for crystalline solids) [2].

This data still contains substantial uncertainty and there are discrepancies with experimental measurements. One approach to refine the data is using a stochastic methodology called Total Monte Carlo (TMC) to randomly perturb key parameters in the TSL data and benchmark each against integral experimental data. This approach has been applied to cross sections of several isotopes as well as TSL data with criticality benchmark experiments from the International Criticality Safety Benchmark Evaluation Project (ICSBEP) and a few small reactors [3,4].

This work contains a similar approach by perturbing TSL data for H in H_2O and benchmarking the data against experimental data obtained from the Open Pool Australian Light Water (OPAL) Reactor, Sydney, Australia. A large set of data with key parameters perturbed in-line with experimental uncertainties were used in reactor simulations of the OPAL reactor using the continuous-energy Monte Carlo reactor physics code Serpent. Two cycles of the OPAL operational history were examined: a fresh core and a typical operational (equilibrium) core. Estimations of uncertainty are then made on several integral quantities, such as k_{eff}, point kinetics parameters and specific reaction rates.

II. BACKGROUND AND METHODOLOGY

At low energies (order of 1eV and less), neutron scattering in H_2O cannot be accurately modeled using the free-gas approximation, owing to the similarly-sized neutron wavelength, molecular bond lengths and intermolecular phenomena. This influences the secondary neutron energy and angle distributions, requiring a more rigorous treatment in data preparation. The double-differential cross section for thermal neutron scattering in solids, liquids or gases is given by:

$$\frac{d^2\sigma}{d\Omega dE'} = \frac{\sigma_b}{4\pi kT}\sqrt{\frac{E'}{E}}e^{-\frac{\beta}{2}}S(\alpha,\beta) \qquad (1)$$

E, E', Ω and Ω' are the incident and secondary energies and angles, σ_b is the bound scatterer cross section, kT is the temperature (in eV) and $S(\alpha,\beta)$ is the symmetric thermal scattering law.

1. Thermal Scattering Law

The basis of thermal scattering cross section treatment comes from the $S(\alpha,\beta)$ data, which needs to be computed. NJOY [5] is a nuclear data processing code, widely used to process and treat nuclear data as well as formatting the data into a form accepted by a neutron transport code. One module of NJOY, called LEAPR, is used to prepare the thermal scattering law. This module receives relevant data for calculating this law, such as the scatterer(s) cross section(s), a continuous phonon distribution, discrete oscillators, various weights for the different modes of freedom of the material and specification of energy (β) and momentum (α) transfer grids. In H_2O, the phonon spectrum is composed of a continuous distribution of broad hindered rotational modes, translational modes and two discrete oscillators corresponding to O-H bond stretching and scissoring (bending) [6]. Fig. 1 shows two different continuous distribution spectra of H_2O that have been used in compiling thermal scattering data in modern nuclear data libraries. Once calculated, the data can be passed on to other NJOY modules (i.e. THERMR) for further processing. At the end of the process chain, thermal scattering cross sections can be produced in ACE format, suitable for use in Monte Carlo codes, such as MCNP or Serpent.

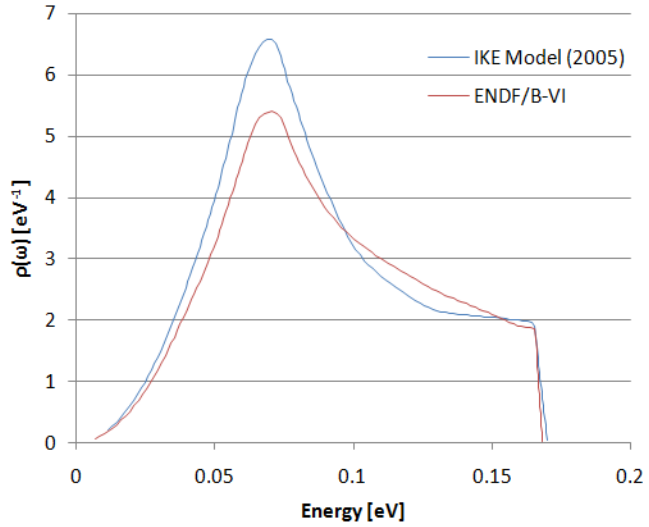

Fig. 1. Continuous distribution of phonon spectrum of H_2O from the IKE model, used in ENDF/B-VII and JEFF-3.1.1 and the older ENDF/B-VI model. Not shown here are the narrow discrete oscillator peaks located around 0.205 and 0.436eV.

2. Uncertainty and Total Monte Carlo Approach

While uncertainties generated in stochastic reactor simulations are quite comprehensive, with standard or relative errors accompanying most calculated parameters, the uncertainty in the underlying data used in such calculations is often not considered. One of the cornerstones of transport calculations is the nuclear data used to determine particle interactions; for example, a neutron-nucleus reaction necessarily requires both the description of the physics of the interaction given by a series of expressions derived from nuclear theory and data that is used to populate the expressions with real-world quantities. Unfortunately, the contribution that data uncertainties impose on a given calculated quantity is unknown upon completion of a typical reactor simulation calculation. This ambiguity shrouds the validity of the output in doubt.

One approach to easily estimate the inherent error associated with the nuclear data used in reactor simulations is by quantifying the effect that varying the parameters that are used in its creation [7]. For example, a given parameter A_i used in the preparation of the thermal scattering law $S(\alpha,\beta)$ can be randomly perturbed then employed in a reactor simulation. Upon completion of the calculation, a quantity q_i can be observed, e.g. k_{eff}. If n randomly perturbed data sets are used in the same simulation scenario, then a distribution of the error that those perturbations produce can be obtained; if the resultant distribution is Gaussian, then the effect can be characterized by the central value $\bar{q}$ and the standard error $\sigma_A(q)$ [8]. However, when using a stochastic calculator each q_i calculated will have its own associated error $\sigma_{i,stat}$ that must be accounted for when interpreting the distribution of q. This approach is called Total Monte Carlo (TMC) and the flow chart of the process is given in Fig. 2.

The input data for the nuclear processing codes is obtained from nuclear models built from fundamental theory and experimental measurements; herein lies the uncertainty of interest in this work. The nuclear models can provide both key parameters used to process cross section data and uncertainties pertaining to them, as a result of measurement precision or model assumptions and limitations. The latter can be randomly sampled and used to modify the former. This process is repeated n times, producing n cross section libraries and a simulation can be run n times. If n is large enough (typically 500-1000), then a reasonable distribution of q can be obtained.

It is necessary to separate the statistical uncertainty from each run from the systematic uncertainty from the perturbations. The observed standard error σ_{obs} is obtained from the distribution of q. The average statistical variance is obtained by:

$$\bar{\sigma}^2_{stat} = \frac{1}{n}\sum_{i=1}^{n}\sigma^2_{i,stat} \qquad (2)$$

The data A error $\sigma_A(q)$ can then be obtained from:

$$\sigma_A(q) \cong \sqrt{\sigma^2_{obs} - \bar{\sigma}^2_{stat}} \qquad (3)$$

Equation 3 holds for $\bar{\sigma}_{stat} \ll \sigma_{obs}$; as the statistical error becomes negligible, the observed error is dominated by the error induced from the perturbed data.

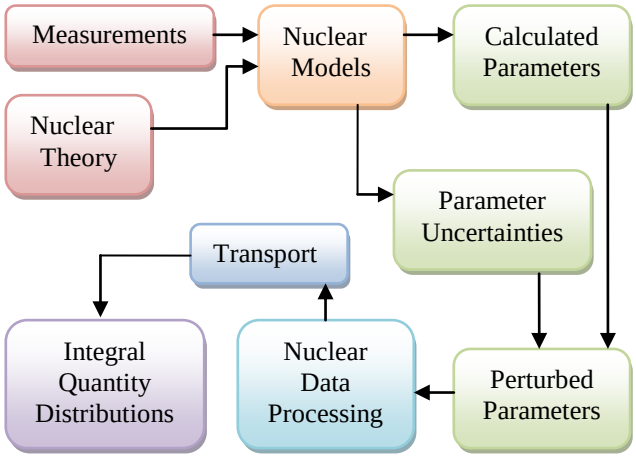

Fig 2. Flow chart of the TMC process. Starting with fundamental theory and measurements, nuclear models are obtained which are used to calculate input parameters for nuclear processing codes, such as NJOY, and their associated uncertainties. Uncertainties can be used to perturb the data, which is then fed into a transport code to calculate integral quantities. The resulting distribution of a given quantity can be used to estimate the uncertainty error induced from the nuclear model uncertainties.

3. Perturbation of the Thermal Scattering Law

Initially, 800 separate cases were run using perturbed H in H_2O data and 300 cases using perturbed D in D_2O data. The data was obtained from the TENDL website, part of the TALYS Project. The details of the data production can be found in [9]. It should be noted, however, that the distribution about the nominal value, from which a new value was sampled, for a given parameter was somewhat arbitrary and the results from this work should be viewed as demonstrating the potential for both the method and as a bounding case of the impact that the perturbations may provide. Both perturbations to H in H_2O and D in D_2O were used in this work and the results are given in Section III.

Following this bounding case was the use of a second set of perturbed data, generated using uncertainties induced from experimental corrections employed in generating cross sections. Total cross section data for H_2O from the EXFOR database was taken and converted into transmission data. The CONRAD code [10] was used to produce uncertainties for a number of LEAPR parameters, a module of NJOY. These parameters were then perturbed accordingly to the computed uncertainties and 1,000 new thermal scattering files were produced. This data is more reflective of the nature of the ambiguity present in modern thermal scattering data. The data was perturbed and generated from the JEFF-3.1.1 library, which employs the IKE model, originally developed in 2005 [6]. A limitation of this model is the lack of diffusion of water molecules; H_2O forms a pseudo-lattice-like structure and particles can diffuse as is typical of most liquids (classic) or jump to new positions in a fashion congruent with solids. Jump-diffusion models, such as the CAB model [11], are presently being developed for H_2O from molecular dynamics (MD) simulations.

Perturbed parameters from LEAPR include the translational weight, discrete oscillator weights, free atom cross section, the phonon frequency spectrum, oscillator energies and α and β grid values. The parameters perturbed in the TENDL and JEFF-3.1.1 libraries previous mentioned are shown in Table I.

TABLE I. Perturbed LEAPR parameter values used in the TMC thermal scattering data for H_2O, based on the TENDL 2012 (TALYS) and JEFF-3.1.1 (CONRAD) libraries.

LEAPR Parameter	TALYS	CONRAD
Free Atom Cross Section (H)	10%	-
Free Atom Cross Section (O)	15%	-
α and β Grid	25%	-
Translational Weight	25%	12.4%
Phonon Distribution Interval	30%	6.5%
Oscillator 1 Weight	25%	30.0%
Oscillator 2 Weight	25%	15.7%
Oscillator 1 Energy	-	7.3%
Oscillator 2 Energy	-	8.2%
Continuous Distribution Normalisation	-	6.5%

4. OPAL Reactor Model Using Serpent

The OPAL Reactor is a 20MW(th) MTR-type reactor designed and constructed by INVAP and commissioned in 2006, though the scope of objectives of the reactor range much broader than just materials irradiation. This modern research reactor uses 16 plate-type LEU dispersed U_3Si_2 assemblies, cooled by light water (LW) and surrounded by a heavy water (HW) reflector vessel. This reflector vessel contains a number of facilities including a cold-neutron source (CNS), various irradiation facilities for the production of specialised isotopes (such as Mo-99) and materials science, silicon neutron transmutation doping (NTD) systems and five neutron beam tubes that penetrate the vessel and provide neutrons for researchers. Core reactivity is controlled using 5 hafnium control plates. The core provides neutrons to the reflector vessel which diffuses thermalised neutrons to the resident facilities, as well as feeding a fraction back to the core. Fig. 3 shows the radial view of the reflector vessel and Fig. 4 shows the radial view of the core assembly.

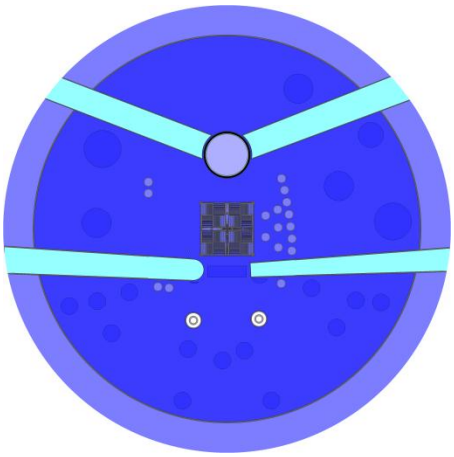

Fig 3. Radial view of the OPAL Reflector Vessel. Present in the model are the core, beam guides, CNS and near-core irradiation facilities.

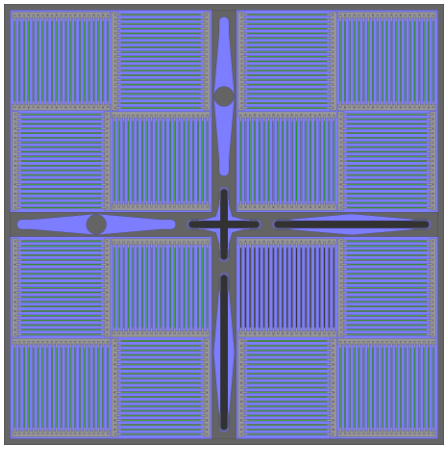

Fig. 4. Radial view of the OPAL core. Shown above are the 16 FAs and 3 of the 5 Hf control blades.

The calculations were carried out using Serpent 2.1.24. The cross section library used was ENDF/B-VII.0, as packaged with Serpent, however the relevant thermal scattering data was substituted in each run. It should be noted that the perturbed thermal scattering data from both the TALYS and CONRAD sets were based the JEFF-3.1.1 evaluation, though previous work has indicated that the calculated k_{eff} is insensitive to the choice in free gas cross sections, a key calculated quantity of interest in this work [12].

The input geometry was written based off data available in the International Atomic Energy Agency (IAEA) Cooperative Research Project (CRP) 1496 in which participants benchmarked reactor physics codes against experimental data available from several research reactors around the world. Within this data were a number of critical configurations of OPAL from prior to Cycle 007, specifying the control rod positions. One position was selected that resembled a control rod configuration typical of coming up to power in the reactor. Each fuel assembly was fresh. An equilibrium cycle (Cycle 019) was also used for the CONRAD data calculations to provide estimation of uncertainties with a typical core loading and obtain additional quantities, as discussed in Section III.

III. RESULTS

1. TENDL Random H_2O and D_2O files

800 files containing perturbed H in H_2O data and 300 files containing perturbed D in D_2O are used. The primary quantity of interest is k_{eff}; the distribution of k_{eff} for the perturbed D in D_2O is shown in Fig. 5 and H in H_2O in Fig. 6 in Section III.2, alongside the CONRAD results. Owing to the arbitrary nature of the random perturbations, these results serve more as a bounding case. Each calculation took approximately 105 minutes, using 64 OMP threads at 2.5GHz, 10^8 neutron histories over 1000 active cycles and 50 inactive cycles for source convergence. The Δk_{eff} was a max of 10pcm for each simulation.

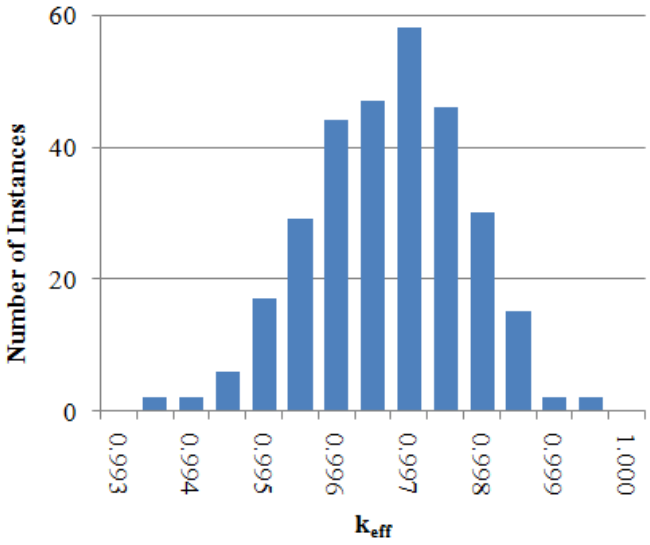

Fig. 5. Distribution of k_{eff} obtained from the 300 TENDL randomly perturbed data for D in D_2O.

Table II describes the distributions for the perturbed H_2O and D_2O runs. As the perturbed H_2O distribution does not conform to a Gaussian shape, the standard error should not be trusted – given the rather uniform-like distribution, as shown in Fig 6., the standard error would be greatly inflated. The perturbed D_2O distribution does look Gaussian, though the uncertainty is relatively small. Despite the low LW inventory in the OPAL core, only an estimated 30% of fission occurs from neutrons reflected from the HW vessel, affirming the higher sensitivity of the system to perturbations in LW cross sections.

TABLE II. Basic statistics from the k_{eff} distributions using perturbed H in H_2O and D in D_2O TSL

Parameter	H in H_2O	D in D_2O
Mean k_{eff}	0.99343	0.99571
σ_{obs} [pcm]	**288.18**	105.64
$\bar{\sigma}_{stat}$ [pcm]	9.96	9.94
$\sigma_A(k_{eff})$ [pcm]	**278.22**	95.70
$\bar{\sigma}_{stat}$ / σ_{obs}	**0.035**	0.094
JEFF-3.1 S(α,β) k_{eff}	0.99370	

All bin widths on any distribution presented in Section III are at a minimum the size of the respective $\bar{\sigma}_{stat}$.

2. CONRAD Random H_2O for Fresh Core

1,000 files obtained from the NEA WPEC-SG42 website containing perturbed H_2O thermal scattering data were used in the same configuration as Section III.1. The parameters perturbed in this data is in accordance with the experimental uncertainties determined from nuclear data from the EXFOR database, as shown in Table I. Consequently, the distribution of instances of a given integral quantity calculated should reflect the net effect that these uncertainties have on the system. The normalization of the calculated quantities reflects the system power level of 36kW.

Fig. 6 shows the k_{eff} distributions from both the TALYS and CONRAD data. The range of the two distributions is comparable, though the CONRAD data produces a Gaussian profile, as does the ^{238}U capture rate in Fig.7 and the total flux leakage rate in Fig. 8. Table III contains the pertinent statistical information for these three calculated quantities. Also included in Table III is the same information about the ^{235}U fission rate, though the statistical and observed errors are near unity that the result can be discarded as trivial.

The range of calculated k_{eff} values can be justified by the strong anti-correlation with the ^{238}U capture rate, as shown in Fig. 9 and the leakage rate, shown in Fig. 10. No other actinides are present, nor is Xe-135 at an equilibrium level, though it does likely contribute. Also not examined is the Cd-113 capture rate, as Cd wires are placed parallel to the fuel plates on 9 of the 16 FAs in the fresh core configuration. The uncertainty in ^{238}U capture is small but may have a knock-on effect on ^{239}Pu production.

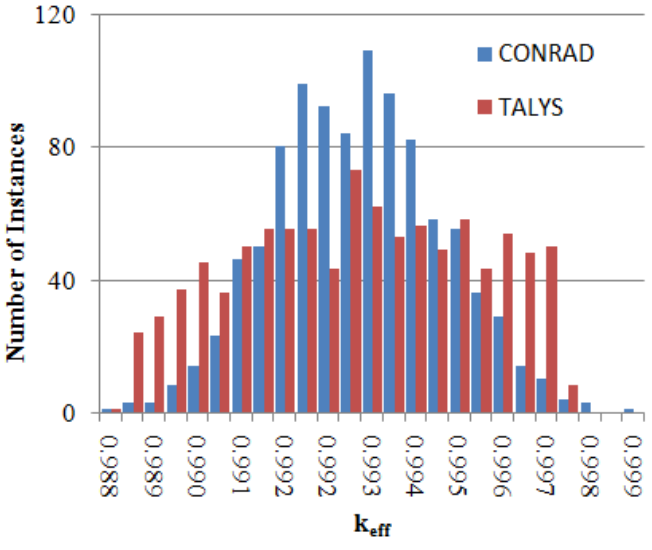

Fig. 6. Distribution of k_{eff} using the TALYS and CONRAD data at the beginning of a fresh cycle.

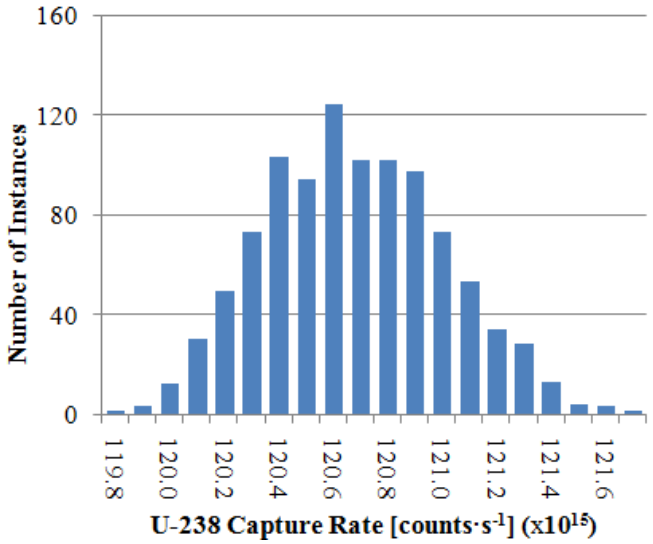

Fig. 7. Distribution of integral ^{238}U capture reaction rate using the CONRAD data at the beginning of a fresh cycle.

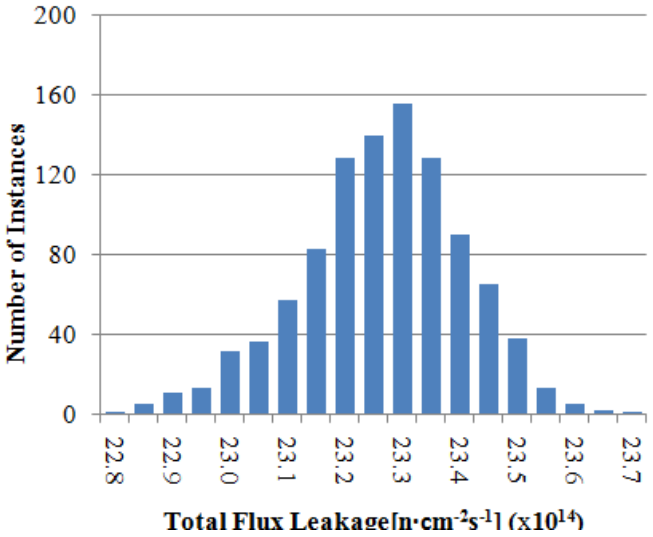

Fig. 8. Distribution of integral neutron flux leakage rate using the CONRAD data at the beginning of a fresh cycle.

TABLE III. Statistical parameters from the integral quantities calculated from the fresh core scenario.

Parameter	k_{eff}	$^{235}U_{fiss}$	$^{238}U_{capt}$	Leakage
Mean k_{eff}	0.99321	1.11e+16	1.21e+15	2.32e+14
σ_{obs} [pcm]	190.2	1.07e+12	3.30e+12	1.42e+12
$\bar{\sigma}_{stat}$ [pcm]	10.0	1.01e+12	5.85e+11	2.53e+11
$\sigma_A(k_{eff})$ [pcm]	189.9	**3.34e+11**	3.25e+12	1.40e+12
$\bar{\sigma}_{stat}$ / σ_{obs}	0.057	**0.95**	0.18	0.18
Relative Induced Error	0.191%	**0.003%**	0.269%	0.603%

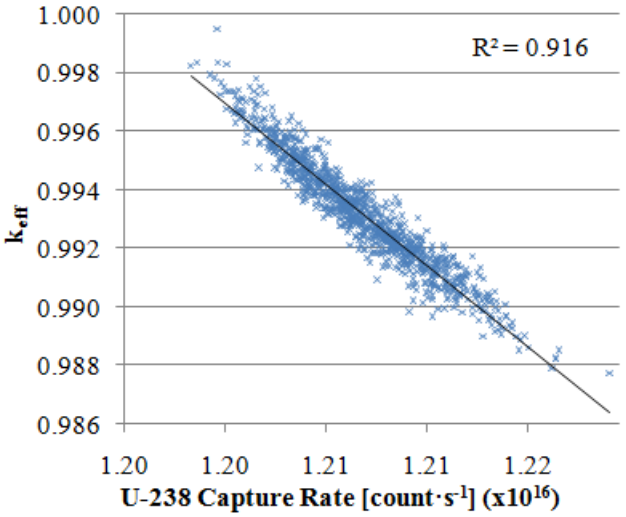

Fig. 9. Scatter plot and regression line of k_{eff} vs. ^{238}U capture rate using the CONRAD data at the beginning of a fresh cycle.

Less obvious is the reasonable correlation between leakage and ^{238}U capture, shown in Fig. 11. This is likely due to another sensitivity, such as Cd or Xe capture. In future work, these reaction rates will be examined.

3. CONRAD Random H_2O during middle of equilibrium cycle

The same 1,000 files used in Section III.2 were used during the middle of an equilibrium cycle. The middle of the cycle was chosen as the power level had been steady for several days and fresh FAs deployed at the start of the cycle have the bulk of their Cd depleted and some ^{239}Pu has been bred. The power level in the simulations was set to 17.77MW and calculated quantities are normalized accordingly. The mean statistical error on k_{eff} for these

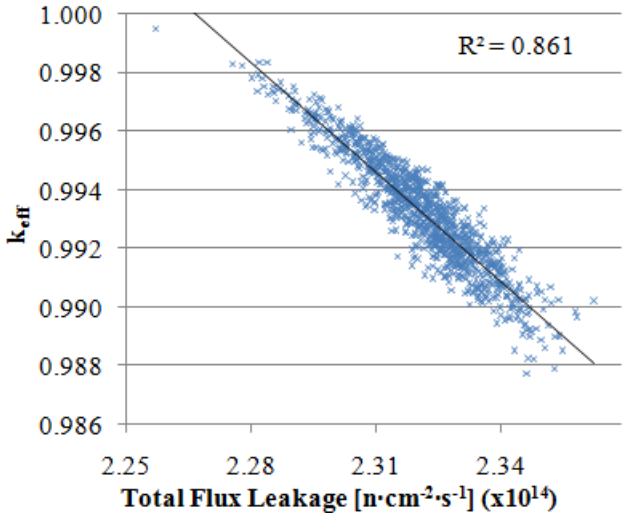

Fig. 10. Scatter plot and regression line of k_{eff} vs. total flux leakage rate using the CONRAD data at the beginning of a fresh cycle.

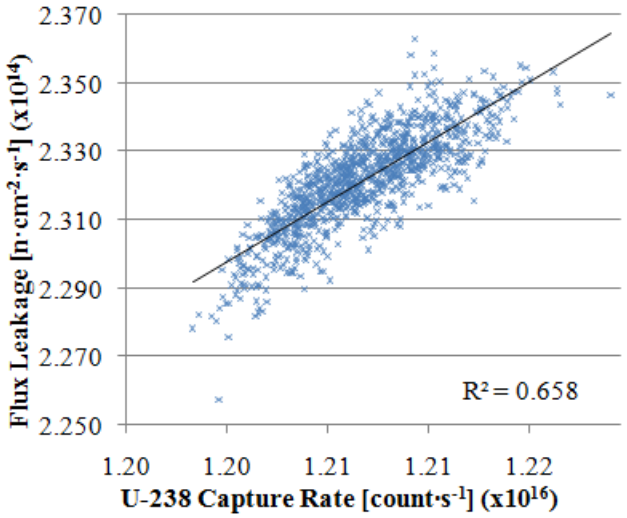

Fig. 11. Scatter plot and regression line total flux leakage vs. ^{238}U capture rate using the CONRAD data at the beginning of a fresh cycle.

simulations is 21 pcm, double that of the calculations in Section III.2. The penalty of larger statistical errors was balanced by the reduction in computation time; further analysis can be conducted if finer control over the uncertainties is required.

Fig. 12 shows the k_{eff} distribution obtained by using the CONRAD data. Note the twin-peaked distribution, a feature also present in Fig. 6. This is possibly two discrete distributions superimposed next to each other. The observed error between k_{eff} shown in Fig. 6 and Fig. 12 are close, though the equilibrium cycle shows a slight reduction.

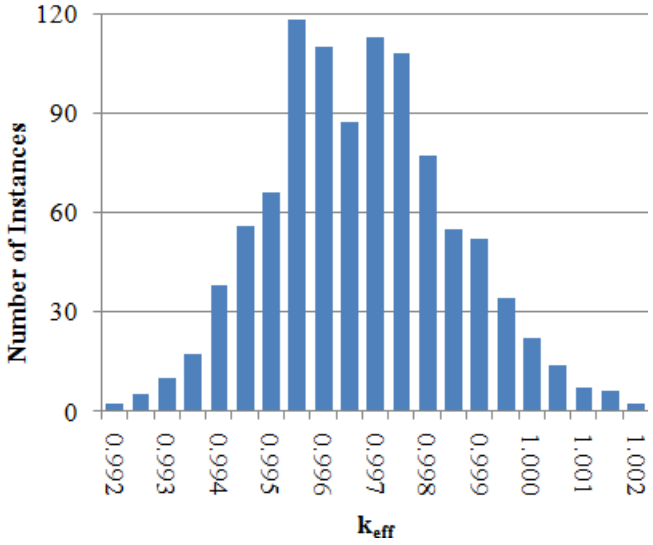

Fig. 12. Distribution of k_{eff} using the CONRAD data mid-cycle during Cycle 019.

The ^{238}U capture rate distribution is shown in Fig. 13. The data-induced relative error between the fresh and equilibrium core calculations is very similar, though the anti-correlation to k_{eff} does weaken somewhat, shown in Fig. 15. Due to the appreciable burnup of the core, the ^{239}Pu fission rate was calculated and the distribution is shown in Fig. 14. Not surprisingly, the ^{239}Pu fission rate was quite sensitive to the thermal scattering perturbations, with the highest relative data-induced error in this work; this is likely due to the low-energy resonance at 0.3eV. The anti-correlation between k_{eff} and the ^{239}Pu fission rate is very strong, as shown in Fig. 16. The correlation in Fig. 17

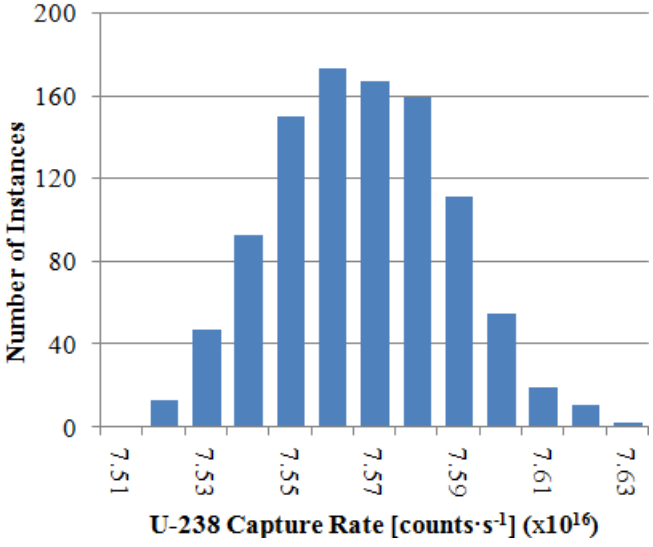

Fig. 13. Distribution of the integral ^{238}U capture reaction rate using the CONRAD data mid-cycle during Cycle 019.

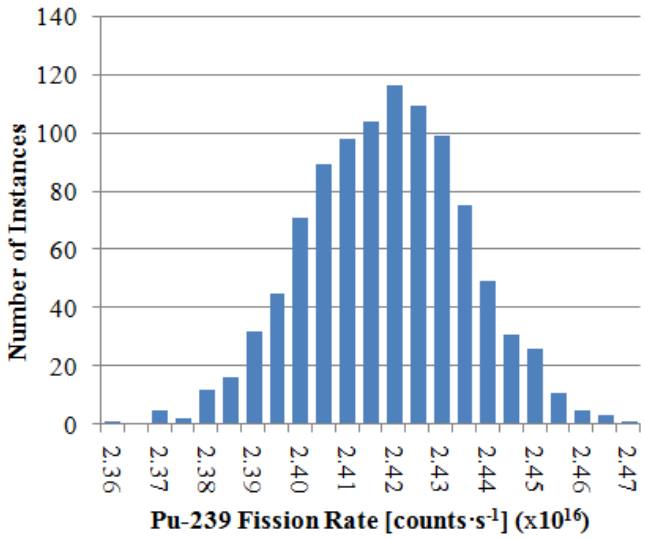

Fig. 14. Distribution of the integral ^{239}Pu fission reaction rate using the CONRAD data mid-cycle during Cycle 019.

between ^{238}U capture and ^{239}Pu fission suggests a different steady state of inventory and fission from ^{239}Pu might be applicable for a given power level, depending on the data set used. However, while the sensitivity of ^{239}Pu fission is relatively high, the inventory in the OPAL reactor at any given time is typically no higher than about 5% of total fissile inventory. Nevertheless, an OPAL FA also undergoes a relatively high burnup, so further analysis could be undertaken using select perturbed thermal scattering data in burn-up simulations. Table IV contains the relevant statistical data about these distributions.

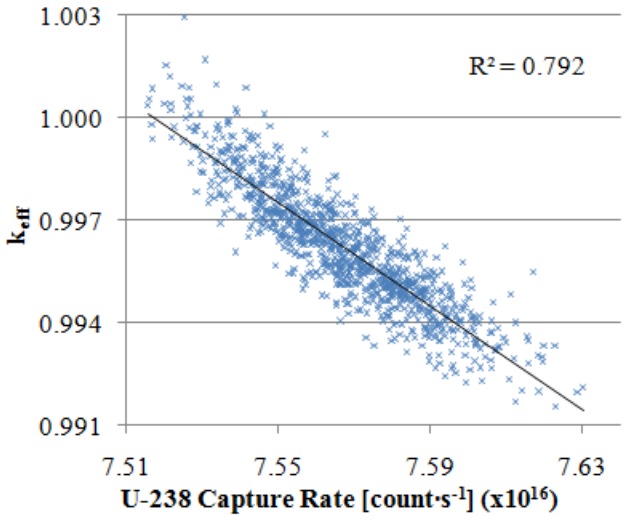

Fig. 15. Scatter plot and regression line of k_{eff} vs. ^{238}U capture rate using the CONRAD data mid-cycle during Cycle 019.

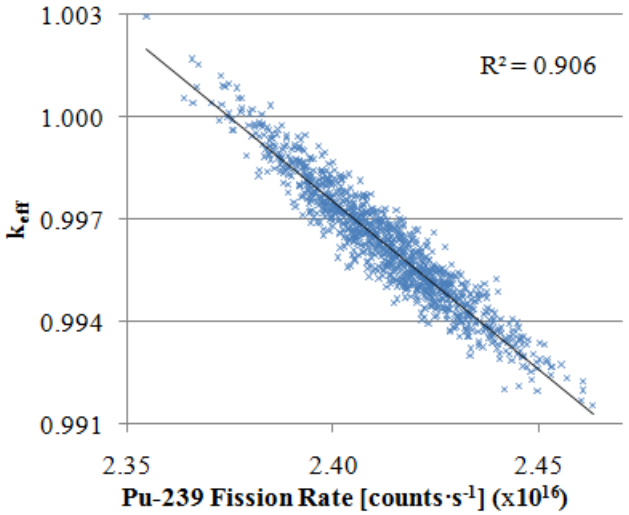

Fig. 16. Scatter plot and regression line of k_{eff} vs. ^{239}Pu fission rate using the CONRAD data mid-cycle during Cycle 019.

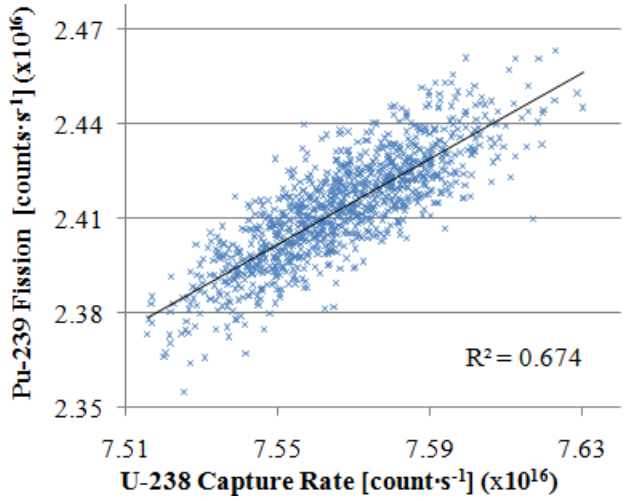

Fig. 17. Scatter plot and regression line of ^{239}Pu fission vs. ^{238}U capture rates using the CONRAD data mid-cycle during Cycle 019.

Additionally, the delayed neutron fraction β_{eff} and the mean prompt neutron lifetime l were also calculated, however the thermal scattering data-induced errors appeared to be negligible, with $\bar{\sigma}_{stat} / \sigma_{obs} > 0.95$, thus they were omitted from this work.

Fig. 18 shows the convergence of the observed errors from each of the measured quantities as a function of the number of runs incorporated into the distribution. While the errors are truly converged by the end of the 1,000 runs, all the curves appear to settle by the 400 mark; future efforts may use a smaller sample size.

TABLE IV. Statistical parameters from the integral quantities calculated during the equilibrium cycle scenario.

Parameter	k_{eff}	$^{235}U_{fiss}$	$^{238}U_{capt}$	$^{239}Pu_{fiss}$
Mean k_{eff}	0.99624	5.19e+17	7.57e+18	2.41e+16
σ_{obs} [pcm]	177.1	2.20e+14	2.07e+14	1.71e+14
$\bar{\sigma}_{stat}$ [pcm]	21.2	1.26e+14	7.57e+13	4.07e+13
$\sigma_A(k_{eff})$ [pcm]	175.9	1.80e+14	1.93e+14	1.66e+14
$\bar{\sigma}_{stat} / \sigma_{obs}$	0.12	0.57	0.37	0.24
Relative Induced Error	0.177%	0.035%	0.255%	0.690%

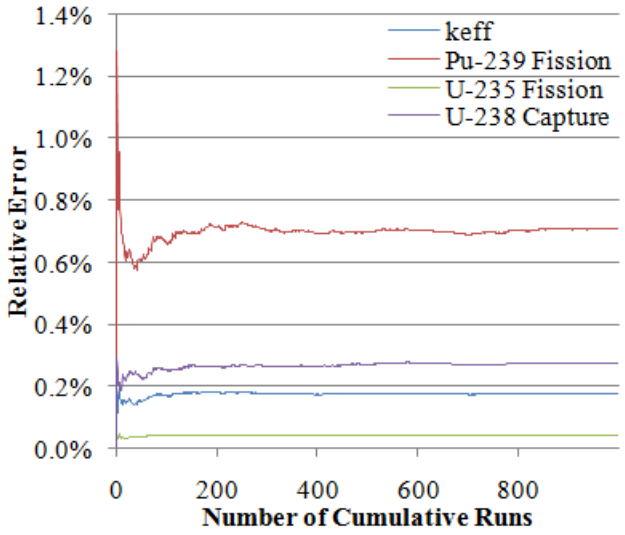

Fig. 18. Convergence of σ_{obs} as a function of the number of cumulative runs from the mid-cycle calculation. All quantity errors converged by the end of the 1000 runs.

IV. CONCLUSIONS

1100 simulations of the OPAL reactor using randomly perturbed thermal scattering data from the TENDL2012 Project was performed. Serpent 2.1.24 was used to simulate a given historical configuration of the OPAL reactor using theis data, yielding distribution of k_{eff} values. The data was generated to provide to scope a potential source for uncertainty and using it may allow researchers to determine whether further work is warranted. It has been established that k_{eff} is sensitive to these parameters and further work was undertaken to better evaluate uncertainties in modern nuclear data.

A new set of random data is available through the Nuclear Energy Agency (NEA) Working Party on International Nuclear Data Evaluation Co-operation

(WPEC), subgroup 42. These files contain perturbations reflective of the experimental uncertainty pertaining to each parameter. In this work, these data were employed in a similar fashion to the TENDL2012 data, both in the same fresh core configuration and an equilibrium core. Integral quantities were calculated including k_{eff}, neutron leakage and various reaction rates. As each distribution conformed to a Gaussian profile, the uncertainty as a result of the data perturbation on each quantity was calculated and presented. Of interest were the distributions for k_{eff}, the ^{238}U capture rate, the ^{239}Pu fission rate and the strong correlations between each them. These actinide reaction rates may have more dramatic implications as a function of time.

Further analysis could be undertaken by:

- Including more pertinent reactions, such as Xe-135 and Cd-113.
- Investigating a subset of perturbed data in burnup calculations to further evaluate the implications of actinide reaction uncertainties.
- Investigate newer models for H_2O, such as the new model [11] from Centro Atomico Bariloche (CAB) which features a jump-diffusion behavior of the water molecules, calculated from molecular dynamics (MD) simulations. Such models could be both more accurate for calculations and be perturbed for propagating uncertainties in a similar fashion to this work.

REFERENCES

1. D.E PARK et al, *Slow Neutron Scattering and Thermalisation*, p. 15, 1st Ed., W. A. Benjamin, Inc., New York, New York (1970).
2. R. E. MACFARLANE, "New Thermal Neutron Scattering Files for ENDFB-VI Release 2", LANL-1994, Los Alamos National Lab (1994).
3. D. ROCHMAN, A. J. KONING, S. C. VAN DER MARCK, "Uncertainties for criticality-safety benchmarks and keff distributions," *Annals of Nuclear Energy*, **36**, 810-831 (2009).
4. E. ALHASSAN et al., "On the use of integral experiments for uncertainty reduction of reactor macroscopic parameters within the TMC methodology," *Progress in Nuclear Energy*, **88**, 43-52 (2016).
5. D. W. MUIR et al., *The NJOY Nuclear Data Processing System, Version 2012*, p. 25, A. C. KAHLER, Ed., Los Alamos National Laboratory, Los Alamos, New Mexico (2012).
6. M. MATTES, J. KEINERT, "Thermal Neutron Scattering Data for the Moderator Materials H2O, D2O and ZrHx in ENDF-6 Format and as ACE Library for MCNP(X) Codes," INDC(NDS)-0470, IKE (2005).
7. A. J. KONING, D. ROCHMAN "Towards sustainable nuclear energy: Putting nuclear physics to work", *Annals of Nuclear Energy*, **35**, 2024–2030 (2008).
8. D. ROCHMAN et. al., "Efficient Use of Monte Carlo: Uncertainty Propagation", *Nuclear Science and Engineering*, **177**, 337–349 (2014).
9. D. ROCHMAN, A. J. KONING, "Random Adjustment of the H in H2O Neutron Thermal Scattering Data," *Nuclear Science and Engineering*, **172**, 287-299 (2012).
10. P. ARCHIER et al., "CONRAD Evaluation Code: Development Status and Perspectives", *Nucl. Data Sheets*, **118**, 488 (2014)
11. J. I. MARQUEZ DAMIAN, J. R. GRANADA, D. C. MALASPINA, "CAB models for water: A new evaluation of the thermal neutron scattering laws for light and heavy water in ENDF-6 format," *Annals of Nuclear Energy*, **65**, 280-289, American Nuclear Society (2014).
12. L. MAUL et al., "OPAL Reactor Calculations Using Reactor Physics Code Serpent," *In proc. PHYSOR 2016*, Sun Valley, ID, May 1-6, American Nuclear Society (2016).